A&A 448, 689–695 (2006)
DOI: 10.1051/0004-6361:20053331

Astronomy & Astrophysics

Discovery of solar-like oscillations in the red giant ε Ophiuchi⋆

J. De Ridder[1], C. Barban[1], F. Carrier[2], A. Mazumdar[1], P. Eggenberger[2], C. Aerts[1], S. Deruyter[3], and J. Vanautgaerden[1]

[1] Instituut voor Sterrenkunde, Katholieke Universiteit Leuven, Celestijnenlaan 200 B, 3001 Heverlee, Belgium
e-mail: joris@ster.kuleuven.ac.be
[2] Observatoire de Genève, 51 chemin des Maillettes, 1290 Sauverny, Switzerland
[3] Sterrenkundig Observatorium, Universiteit Gent, Krijgslaan 281 S9, 9000 Gent, Belgium

Received 28 April 2005 / Accepted 24 October 2005

ABSTRACT

We present the discovery of solar-like oscillations in time-series of the G9.5 red giant ε Ophiuchi. The data were obtained with the CORALIE spectrograph at the 1.2 m Swiss telescope in La Silla and the ELODIE spectrograph at the 1.93 m telescope at the Observatoire de Haute Provence. Periodic variations can be observed in the radial velocity time series of individual nights. In the power spectrum of the radial velocity time series there is a clear power excess around 60 μHz, and several individual oscillation frequencies can be distinguished. Our auto-correlation and comb response analysis reveals a large separation of either 4.8 μHz or (its 11.57 μHz alias) 6.7 μHz. We estimate the position of ε Oph in the HR diagram, and verify whether CESAM shell hydrogen-burning stellar models exist that can reproduce the observed frequency separation.

Key words. stars: oscillations – stars: individual: HD 146791 – stars: late-type

1. Introduction

For years, late-G and early-K red giants have been considered as being pulsationally stable, or at least having only oscillations with amplitudes below the detection threshold (see e.g. Jorissen et al. 1997 and Eyer & Grenon 1997). It is only quite recently that new high-precision time series have allowed detection of towards low-amplitude oscillations in G−K giants. We mention, for example, the detection of low-amplitude oscillations in Arcturus (K1.5III) by Hatzes et al. (1994), in α UMa (K0III) with the WIRE satellite by Buzasi et al. (2000), in GSC09137-03505 (K2.5III) with the Hubble Space Telescope by Kallinger et al. (2005), and in ξ Hya (G7III) with the CORALIE spectrograph by Frandsen et al. (2002). With these clear detections of oscillation signatures, red giant seismology has gained extra momentum.

Theoretical investigations suggest that these low-amplitude oscillations are likely to be solar-like and stochastically excited by turbulent convection, although self-excited Mira-like oscillations cannot always be easily excluded (see Dziembowski et al. 2001). Red giants showing a frequency comb are evidently promising targets to study the interior of evolved stars.

The interpretation of red giant oscillations is still far from straightforward. The less than satisfactory theoretical reproduction of the ξ Hya amplitudes (Houdek & Gough 2002) illustrates some of the problems on the theoretical side. Observationally, only very few long high-precision time series of red giants have been obtained. The few currently available datasets are not able, for example, to allow verification of whether the non-radial modes are so heavily damped that the power spectrum is dominated by radial modes, as predicted by theory (see e.g. Dziembowski et al. 2001; and Christensen-Dalsgaard 2004). In addition, we also have little observational information about the damping times of oscillation modes in red giants. Only one indirect observational attempt has been made to derive the typical damping time τ of the modes of ξ Hya (Stello et al. 2004), resulting in $\tau \approx 2$ days, but no uncertainty or reliability estimate was given.

Evidently, several of the open problems can only be solved by more (and if possible, better) observational time series of red giant oscillations. In this paper, we provide clear evidence for the presence of low-amplitude oscillations in new spectroscopic time series of the G9.5III giant ε Ophiuchi (HD 146791). In Sect. 2, we discuss the time series and the data reduction. An overview of the basic parameters of ε Oph is given in Sect. 3. The frequency analysis is presented in Sect. 4. In Sect. 5, we show that the theoretical models are consistent with the observations, and give our conclusions.

2. Observations and data reduction

In July and August of 2003 we set up a spectroscopic bi-site campaign for the bright stars ε Oph and η Ser. We selected

⋆ Based on observations obtained at the 1.2-m Swiss Euler telescope at La Silla (Chile) and at the 1.93-m telescope at the Haute-Provence Observatory (France).

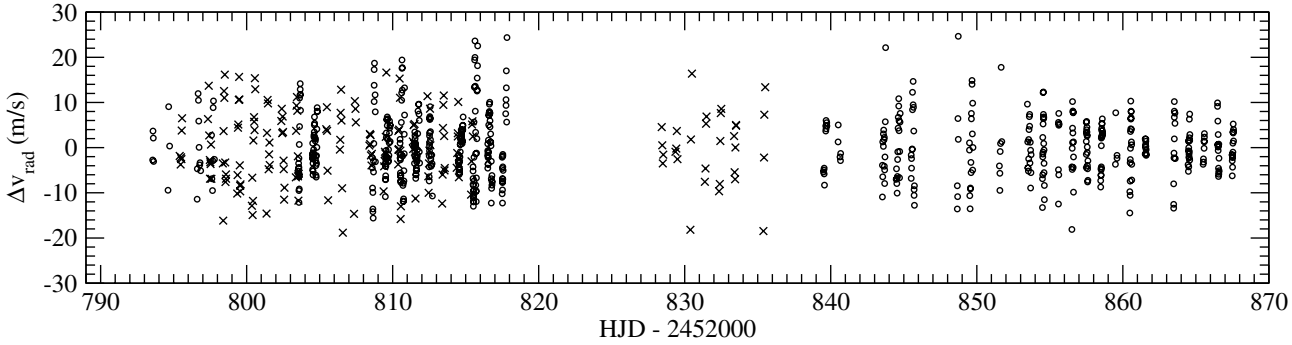

Fig. 1. The radial velocity time series computed with the optimum-weight technique with one reference spectrum per night. The circles and crosses denote the observations made with CORALIE and ELODIE respectively.

these stars because both are slowly rotating and thus narrow-lined red giant stars near the celestial equator. This paper concentrates on ε Oph; the results for η Ser will be discussed in Carrier et al. (2006, in preparation). With the fiber-fed echelle spectrographs CORALIE on the Swiss 1.2 m Euler telescope at La Silla, and ELODIE on the French 1.93 m telescope at the Observatoire de Haute-Provence, we obtained a total of 839 spectra of ε Oph, during 54 nights, and ranging in wavelength from 388 nm to 682 nm. The exposure time was adapted from 180 s to 200 s, depending on the air mass, to get a S/N ratio at 550 nm of at least 100 without averaging out a too large fraction of the pulsation phase. The thorium calibration spectra were recorded simultaneously with the stellar spectrum through a second fibre, in order to guarantee a highly accurate wavelength calibration.

We considered two options to precisely compute the radial velocity variations. The first option is to cross-correlate each stellar spectrum with a mask, i.e. a template spectrum with box-shaped emission lines at the wavelengths of the absorption lines of interest (see e.g. Baranne et al. 1996). The second option is the more precise optimum-weight method described by Bouchy et al. (2001), which uses a weighted difference between the stellar spectrum and a reference spectrum to compute the Doppler velocities. We found, however, that using only one reference spectrum for the entire dataset did not yield a lower noise level in the power spectrum than with the cross-correlation technique. The reason is that the optimum-weight method assumes no non-linear line-intensity variations as a function of the Doppler shift. This means that for too large Doppler velocity variations, such as the one introduced by the changing motion of the Earth during an observing run, the quality of the resulting time series degrades. As for the red giant ξ Hya (Frandsen et al. 2002), we *did* find a significant improvement of the noise level when we used one reference spectrum per night, for which we took the highest S/N spectrum of that night. Changing the velocity zero point each night implies of course a high-pass filter in the frequency domain: information on long-term variations is unavoidably lost. The time series computed with the optimum-weight method with one reference spectrum per night is shown in Fig. 1. In what follows we will refer to this time series simply as "the" time series.

3. Global stellar parameters

We first give an overview of the basic stellar parameters of ε Oph. This will allow us to locate the star in the HR-diagram. This position and its error box will be useful for the theoretical modeling in Sect. 5 and can be used as an additional constraint for further asteroseismic investigations.

In his catalogue of evolved G and K stars, Taylor (1999) lists the effective temperature $T_{\rm eff} = 4855 \pm 28$ K for ε Oph. On the other hand, the $T_{\rm eff}$ value estimated from the infrared flux method by Blackwell & Lynas-Gray (1998), is 4882 ± 44 K. In the literature we found the Johnson colours $V-K = 2.24 \pm 0.03$ (Taylor 1999) and $B-V = 0.96 \pm 0.01$ (Simbad, CDS). Using the former colour with the calibration of Bessell et al. (1998) leads to $T_{\rm eff} = 4847 \pm 29$ K. The latter colour in combination with the calibration of Flower (1996) gives $T_{\rm eff} = 4920 \pm 25$ K. Using the same colour with the calibration of Houdashelt et al. (2000) gives the very similar value $T_{\rm eff} = 4933 \pm 20$ K. Note that all quoted values deviate less than 50 K from the mean value, which indicates that the random errors are quite small. The final $T_{\rm eff}$ value we adopt is the mean value $T_{\rm eff} = 4887 \pm 100$ K. The uncertainty quoted is more conservative than the ones mentioned before, and tries to incorporate a possible systematic error because of inaccurate stellar atmosphere models. In addition, it is more in agreement with uncertainties of effective temperatures of red giants derived from micro-modeling of ISO-SWS infrared spectra (Decin et al. 2003).

The luminosity can be estimated using the Hipparcos parallax $\pi = 30.34 \pm 0.79$ mas, which leads to a distance of $d = 33.0 \pm 0.9$ pc. Given the visual magnitude of $m_V = 3.24 \pm 0.02$ (e.g. Blackwell et al. 1990), the absolute visual magnitude is therefore $M_V = 0.65 \pm 0.06$. We estimated the bolometric correction BC_V in four different ways. The $T_{\rm eff} - BC_V$ calibration of Flower (1996) gives $BC_V = -0.35 \pm 0.07$. Interpolation in the theoretical tables of Lejeune & Schaerer (2001) leads to $BC_V = -0.33 \pm 0.04$. Interpolation in the theoretical $T_{\rm eff} - BC_K$ tables of Houdashelt et al. (2000) gives $BC_K = 1.91 \pm 0.06$ and thus $BC_V = BC_K - (V-K) = -0.33 \pm 0.07$. The theoretical $BC_K - (V-K)$ calibration of Bessel et al. (1998) implies $BC_K = 1.93 \pm 0.03$ and therefore $BC_V = -0.31 \pm 0.04$. The final value we adopt is $BC_V = -0.33 \pm 0.07$ giving a lower weight to the older calibration of Flower (1996) but

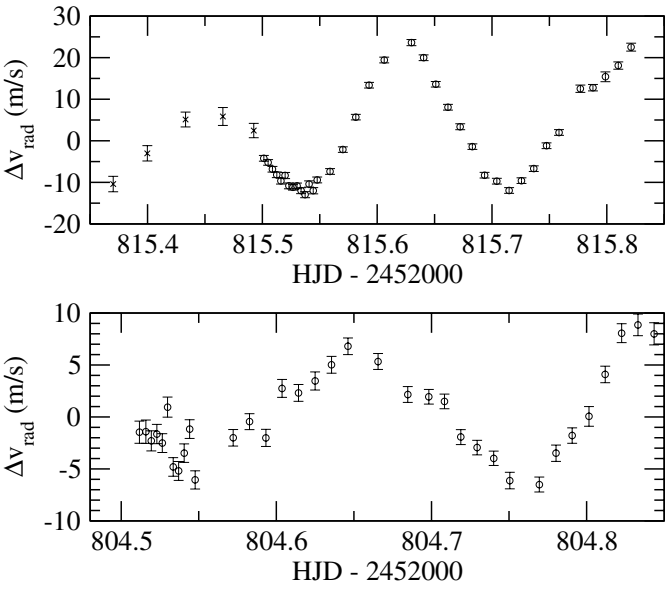

Fig. 2. Radial velocity time series of two particularly good nights, clearly showing the oscillations in ε Oph. The circles and crosses denote the observations made with CORALIE and ELODIE. The error bars shown relate to the photon noise, and are therefore lower limits for the true uncertainty.

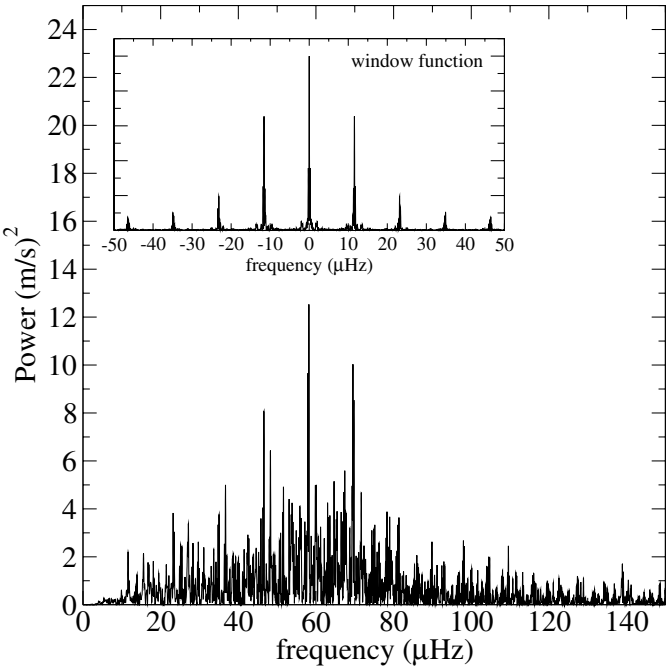

Fig. 3. The power spectrum of the time series of ε Oph shown in Fig. 1. The power excess around 60 μHz is caused by stellar oscillations. Note that the drop in power towards low frequencies is a consequence of choosing a different reference point for each night to compute the time series. The Fourier transform was normalised with a factor $2/N$ where N is the number of data points.

being nevertheless conservative. The absolute bolometric magnitude is therefore $M_{\rm bol} = M_V + BC_v = 0.32 \pm 0.09$. Adopting $M_{\rm bol,\odot} = 4.746$, we thus obtain $L/L_\odot = 59 \pm 5$.

From our CORALIE spectra, we derive $v \sin i = 3.4 \pm 0.5$ km s^{-1}.

4. Data analysis

Our dataset is the first high-precision radial velocity time series of ε Oph, and is also the first dataset to clearly show oscillations. We only know of two other time series: the photometric time series of ε Oph of Percy & Shepherd (1992) and the Hipparcos time series (Perryman et al. 1997). Neither of those two datasets reveal variations. As we will show later, the amplitudes of the oscillations are so small that for both photometric datasets the oscillations were likely hidden in the noise.

The most convincing proof of the presence of oscillations in ε Oph can be seen in the time series themselves. Figure 2 shows the radial velocity variations on two particularly good nights (in the sense of S/N and number of data points), which clearly shows oscillatory behaviour with a frequency around 60 μHz. These oscillations are also seen in the power spectrum, as is shown in Fig. 3. Note that the power spectrum drops to zero at low frequencies. This is a consequence of using a different reference point for each night which implies high-pass filtering, as discussed in Sect. 2. For brevity we do not show the power spectrum of the time series obtained by simple cross-correlation, but it also clearly shows the same oscillation bump around 60 μHz.

A noticeable difference between the power spectrum of ξ Hya presented by Frandsen et al. (2002) and the power spectrum of ε Oph presented in this paper is the presence of a dominant peak in the latter.

In a first analysis we focus on the auto-correlation of the power spectrum to search for a large frequency separation. The auto-correlation of the full power spectrum turns out to be too noisy to reliably extract any frequency spacing apart from the 11.57 μHz caused by the day-night rhythm of the observations. This is shown at the top of Fig. 4. We therefore apply thresholding which implies removing all peaks in the power spectrum lower than a specified threshold T, and computing the auto-correlation with the remaining N peaks. In Fig. 4 we show the auto-correlation for different thresholds in the left panel, and the corresponding thresholded power spectra in the right panel. Changing the threshold from 7 (m/s)^2 to 5 (m/s)^2 we see 5 groups of frequency peaks appear which we have labeled (a) to (e). These peaks gradually merge into each other due to the noise, when the threshold is lowered further to zero. Peak (e) at $\Delta\nu_{\rm e} \approx 11.6\,\mu$Hz, obviously represents the frequency spacing due to one-day aliasing. The other peaks in the auto-correlation ($\Delta\nu_{\rm a} \approx 2\,\mu$Hz, $\Delta\nu_{\rm b} \approx 4.8\,\mu$Hz, $\Delta\nu_{\rm c} \approx 6.5\,\mu$Hz and $\Delta\nu_{\rm d} \approx 9.6\,\mu$Hz) can be related to each other:

$$\Delta\nu_{\rm a} \approx \Delta\nu_{\rm e} - \Delta\nu_{\rm d}$$
$$\Delta\nu_{\rm b} \approx \Delta\nu_{\rm e} - \Delta\nu_{\rm c}$$
$$\Delta\nu_{\rm d} \approx 2\Delta\nu_{\rm b}.$$

This implies that the auto-correlation does not give clear evidence for more than one large frequency separation. Although the frequency separations at $\Delta\nu_{\rm a} \approx 2.0\,\mu$Hz and $\Delta\nu_{\rm d} \approx 9.6\,\mu$Hz appear "first" in Fig. 4, and they are always more pronounced than the peaks at $\Delta\nu_{\rm b} \approx 4.8\,\mu$Hz and $\Delta\nu_{\rm c} \approx 6.5\,\mu$Hz, the following simple simulation indicates that they are likely not genuine

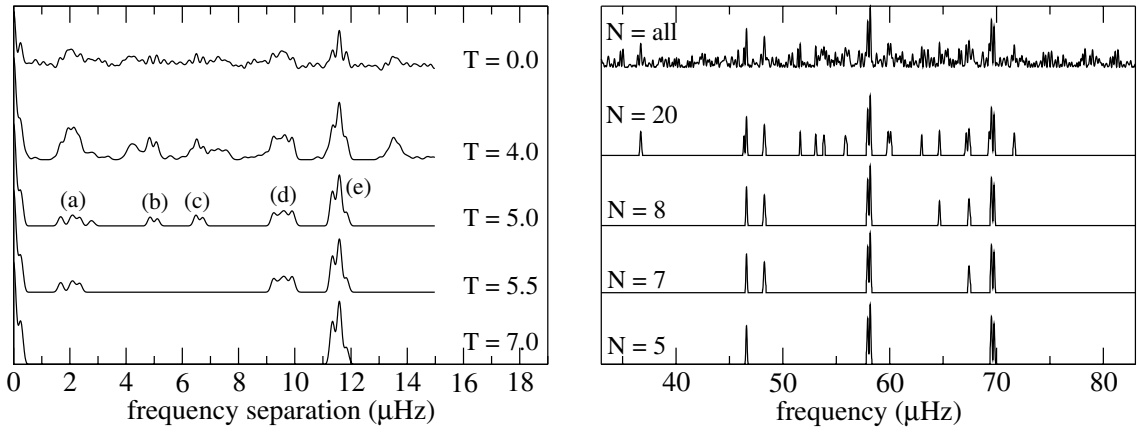

Fig. 4. *The left panel* contains the auto-correlations (in arbitrary units) for different thresholds T, in $(\mathrm{m/s})^2$, computed from the corresponding thresholded power spectra shown in the right panel. Each time the number N of retained peaks is mentioned. Note that some of the peaks are too close to be resolved by eye from this figure. Going from high to low threshold we can gradually see 5 groups (a)−(e) of frequency separations appear in the auto-correlation which then gradually merge into each other due to the noise.

separations but in fact window function aliases. We constructed synthetic time series with exactly the same time sampling as the one of ε Oph, consisting of a sum of 3 sines:

$$y_i = \sum_{k=-1}^{+1} \sin(2\pi(\nu_0 + k\Delta\nu)t_i) \quad (1)$$

where $\nu_0 = 58.2\ \mu$Hz, and where $\Delta\nu$ is either $\Delta\nu_\mathrm{a}$, $\Delta\nu_\mathrm{b}$, $\Delta\nu_\mathrm{c}$ or $\Delta\nu_\mathrm{d}$. For each of these time series we computed the power spectrum and the auto-correlation. The results are shown in Fig. 5. In the cases $\Delta\nu = \Delta\nu_\mathrm{b}$ or $\Delta\nu = \Delta\nu_\mathrm{c}$ we also see auto-correlation peaks at $\Delta\nu_\mathrm{a} \approx 2.0\ \mu$Hz and $\Delta\nu_\mathrm{d} \approx 9.6\ \mu$Hz, confirming that the latter are indeed window function artefacts. The other way around, however, i.e. if $\Delta\nu = \Delta\nu_\mathrm{a}$ or $\Delta\nu = \Delta\nu_\mathrm{d}$, there are no auto-correlation peaks at $\Delta\nu_\mathrm{b} \approx 4.8\ \mu$Hz or $\Delta\nu_\mathrm{c} \approx 6.5\ \mu$Hz. Also the theoretical models of ε Oph (see Sect. 5) confirm that either $\Delta\nu_\mathrm{b}$ or $\Delta\nu_\mathrm{c}$ is more likely to be the true large frequency separation.

In an attempt to choose between $\Delta\nu_\mathrm{b} \approx 4.8\ \mu$Hz and $\Delta\nu_\mathrm{c} \approx 6.5\ \mu$Hz, and to place the frequency comb in the power spectrum, we computed comb responses. We define a comb response $C(\nu_0, \Delta\nu)$ of N peaks around a frequency ν_0 with peak spacing $\Delta\nu$ as

$$C(\nu_0, \Delta\nu) \equiv \frac{1}{N+1} \sum_{k=0}^{N} S(\nu_0 - k\Delta\nu)\, S(\nu_0 + k\Delta\nu) \quad (2)$$

where $S(\nu)$ is the power spectrum. We set $\nu_0 = 58.2\ \mu$Hz, but being conservative in deciding which frequency is genuine and which one is a window function artefact, we also computed comb responses for $\nu_0 = 69.5\ \mu$Hz and $\nu_0 = 46.6\ \mu$Hz. The result for the latter frequency is considerably worse than for the former two, and is therefore omitted here. The responses for $N = 1$, i.e. a triplet, are shown in Fig. 6. For the most dominant peak in the power spectrum, at $58.2\ \mu$Hz, the two candidate frequency separations are roughly the same as we found in the auto-correlation: $\Delta\nu = 6.5\ \mu$Hz and $\Delta\nu = 5.1\ \mu$Hz, with the former being slightly more likely. However, for the second strongest peak in the power spectrum, at $69.5\ \mu$Hz, only the frequency separation of $\Delta\nu = 4.8\ \mu$Hz seems to be relevant.

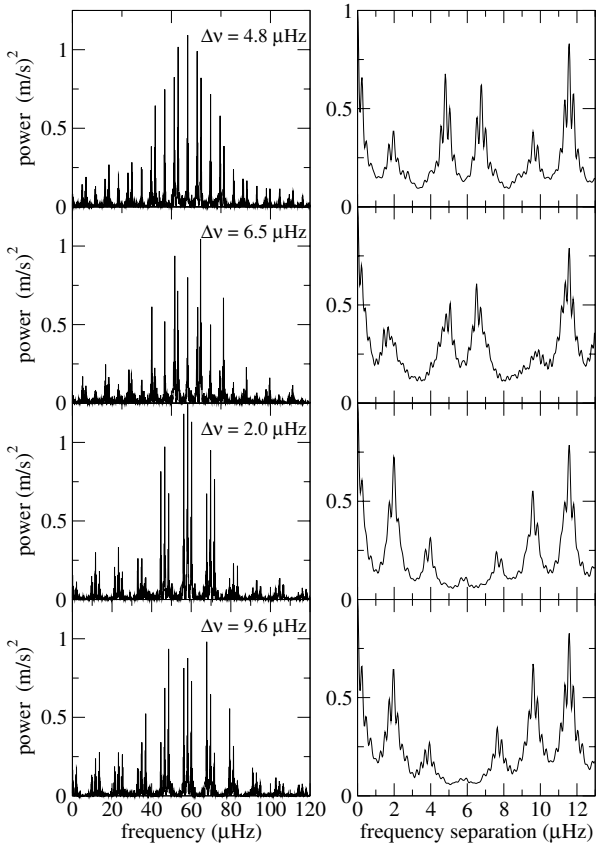

Fig. 5. Power spectra and the corresponding auto-correlations of 4 synthetic time series, described by Eq. (1). The time sampling is the same as the one of ε Oph, and the auto-correlation is computed in the range [30, 90] μHz as for Fig. 4. For each case, the chosen large separation is indicated. Note that most peaks in the power spectra are window aliases.

The comb responses of a quintuplet ($N = 2$) contain more window function artefacts, but the results for the large separation do not change.

Thus, we find observational evidence for one comb of frequency peaks in the power spectrum, but due to one-day

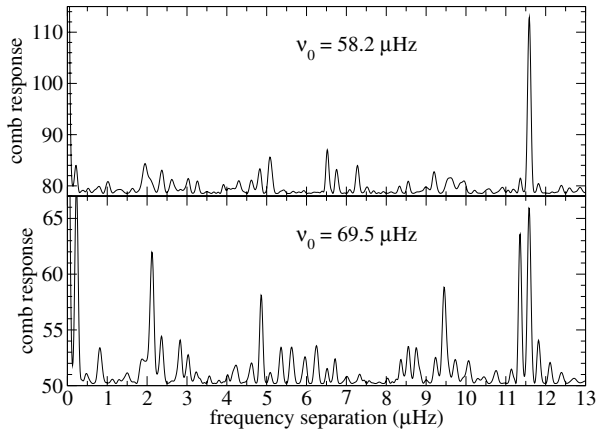

Fig. 6. Comb responses $C(\nu_0, \Delta\nu)$ as a function of the frequency separation $\Delta\nu$, around the frequencies $\nu_0 = 58.2$ μHz (*upper panel*) and $\nu_0 = 69.5$ μHz (*lower panel*). In both cases a triplet response was computed, i.e. $N = 1$ in Eq. (2).

Table 1. Data of the 3 candidate combs. The comb identification number is the same as used in Fig. 7. The "anchor" peaks of the combs are put in boldface.

Comb ID	$\{\nu_n\}$ (μHz)	$\overline{\Delta\nu}$ (μHz)
(1)	{48.3, 53.1, **58.2**, 63.0, 67.4}	4.8
(2)	{51.6, **58.2**, 64.7, 71.7}	6.7
(3)	{59.9, 64.7, **69.5**, 74.4}	4.8

aliasing effects we cannot unambiguously determine which frequencies belong to the comb. We find 3 candidate combs, which we list in Table 1. The frequencies of these combs were determined by locating the positions of the maxima in the power spectrum. We therefore can expect a rather large deviation from the true eigenfrequencies in the case of short damping times. The digit after the point therefore reflects the precision dictated by the total time span of the time series, rather than the accuracy with which the eigenfrequencies were measured. The candidate combs are also indicated on Fig. 7 where we used the same comb identification numbers as in Table 1. From this figure, we can see that the third candidate comb seems to be somewhat less likely than the two other candidate combs. Note that we put regions that are separated in frequency by (a multiple of) the one-day alias 11.57 μHz in the same colour (visible only in the on-line version of the paper). This should make it clear why the peaks at, for example, 36.7 μHz and 79.0 μHz are likely not real eigenfrequencies but rather alias frequencies.

5. Theoretical models

We verified whether a shell hydrogen-burning stellar model exists in a given box in the HR diagram that can reasonably well reproduce the observed frequency separations of ε Oph. To do so we used the CESAM evolutionary code (Morel 1997) to compute the stellar equilibrium models, and the Aarhus adiabatic pulsation code ADIPLS (Christensen-Dalsgaard & Berthomieu 1991) to compute the eigenfrequencies. The computations were made with the OPAL equation of state (Rogers & Nayfonov 2002), the OPAL opacity tables (Iglesias & Rogers 1996) complemented by the low-temperature opacity tables of Alexander & Ferguson (1994), and the standard mixing length theory of convection (Henyey et al. 1965). The reference mixing length value of the present-day Sun is $\alpha_{\rm sun} = 1.8$, measured in units of the local pressure scale height. It is acknowledged that ε Oph might be actually in the slower evolving core helium-burning stage, and future work is foreseen to construct models in this stage of evolution.

The cool effective temperature of ε Oph almost excludes the possibility of the star being in the so-called "dip" phase before ascending the giant branch. We therefore considered only models in the ascending red giant phase. In addition, for each of these models we only considered radial modes, as the oscillation amplitudes of the non-radial modes are expected to be much smaller than for the radial modes (Dziembowski et al. 2001). We constructed a grid of models lying within the error box on the HR diagram (Fig. 8) with different values of stellar parameters. We find that it is possible to construct stellar models that have large separation values fairly close to either of the two candidate derived values (4.8 μHz and 6.7 μHz). The crucial stellar parameter that has to be tuned to match either of these frequency separations turns out to be α, the mixing length of convection. With a value of $\alpha = 1.6$, we could find models with mass $\simeq$2.8 $M_\odot$ that have mean large separations close to 6.7 μHz. Models with a higher value of $\alpha = 1.8$ tend to have smaller separations. Such models with mass $\simeq$1.9 $M_\odot$ match quite well the observed large separation value of 4.8 μHz. We found that the effect of changing the chemical composition is relatively small compared to that of the mixing length. For a given choice of the mean large separation, it is not possible to constrain the metallicity from theoretical models. In what follows the models were computed with an initial metallicity of $(X_0, Z_0) = (0.72, 0.012)$, in agreement with the results of Taylor (1999) who finds [Fe/H] $= -0.12 \pm 0.05$.

The evolutionary tracks of some of our best models are shown in Fig. 8. We also indicate four specific models for which we show in Fig. 9 the large separation $\Delta\nu_n \equiv \nu_n - \nu_{n-1}$ as a function of ν_n in the range of interest, compared with the observations. The theoretical $\Delta\nu$ values fit the observations fairly well. One should keep in mind that changing the exact modeling of the surface layers of the star can result in a significant horizontal shift of the theoretical curves. The theoretical curves show an appreciable variation of $\Delta\nu$ in the frequency range of interest. The fairly large variation in $\Delta\nu$ around 4.8 μHz denoted by the "$\circ$" symbol, is likely not intrinsic, and may be caused by an inaccurate determination of the eigenfrequencies due to short damping times. The quality of the data did not allow us to fit Lorentz profiles which would give a more accurate determination of the oscillation frequency.

Thus, we can find models matching either of the observed values $\Delta\nu = 4.8$ μHz or $\Delta\nu = 6.7$ μHz by changing the mixing length parameter. Since the value of the mixing length is an uncalibrated theoretical parameter, especially for largely convective stars such as red giants, it is not possible to rule out any of the candidate combs from theoretical arguments alone.

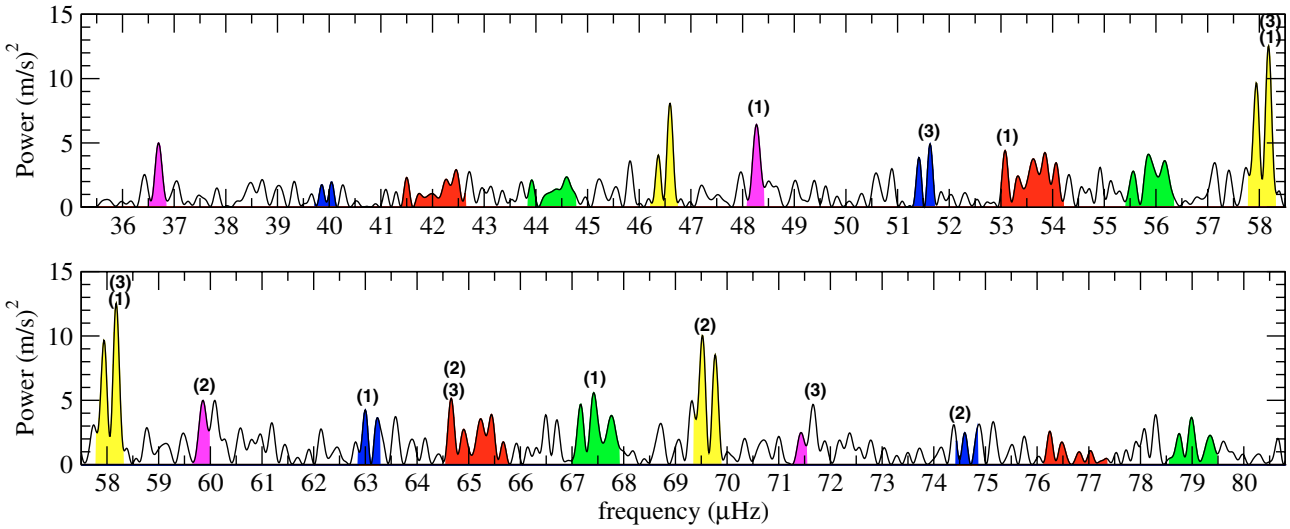

Fig. 7. Power spectrum annotated with possible sets of oscillation peaks. The number above a peak indicates to which candidate comb the frequency belongs (see Table 1). To recognize better which frequencies are alias frequencies of each other, we have put frequency peaks that are separated by (a multiple of) the one-day alias 11.57 μHz in the same colour (visible only in the on-line version of the paper), and this for the 5 most important frequency groups (hence 5 colours).

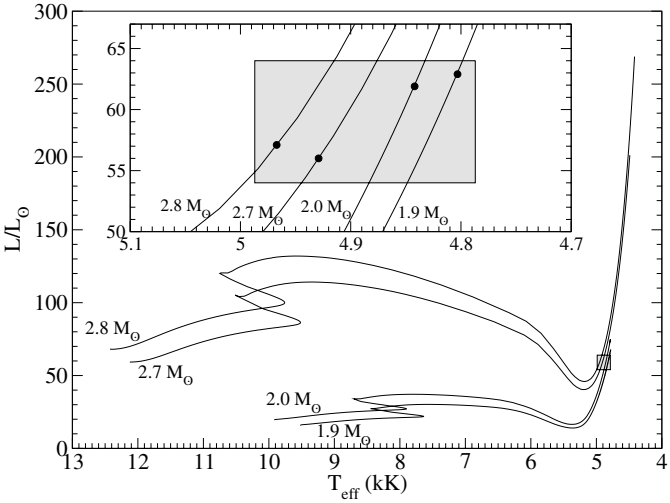

Fig. 8. HR diagram containing the estimated position of ε Oph (grey box) and the evolutionary tracks of some of our best models (solid lines). The inset contains a magnification of the region around the position of ε Oph, and its axes have the same units as the main figure. The four models for which we show the large separation in Fig. 9 are shown in the inset as bullets. The higher mass models (2.7 $M_\odot$ and 2.8 $M_\odot$) were constructed with $\alpha = 1.6$, while the lower mass models (1.9 $M_\odot$ and 2.0 $M_\odot$) were constructed with $\alpha = 1.8$.

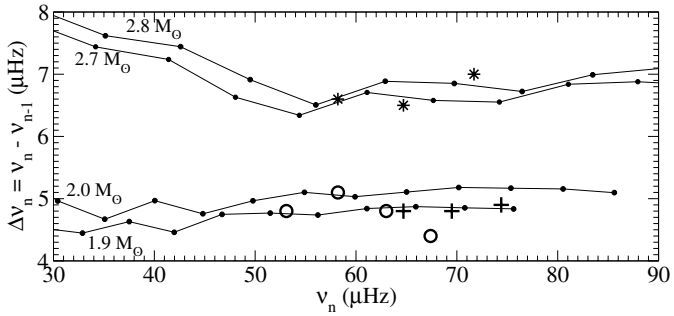

Fig. 9. Comparison between the observed and theoretical large separation $\Delta\nu_n \equiv \nu_n - \nu_{n-1}$ as a function of ν_n. The shown theoretical separations were computed from the radial modes of the four stellar models indicated in Fig. 8, and are connected with solid lines to help guide the eye. The observational separations were computed from the three candidate combs specified in Table 1: open circles correspond to comb (1), asterisks to comb (2) and plus signs to comb (3).

6. Conclusions

We obtained a high-precision radial velocity time series of 839 data points of the red giant ε Oph spread over 75 days. The oscillations are clearly visible in the time series of individual nights (see Fig. 2). The power spectrum shows a significant excess around 60 μHz, with a maximum peak amplitude of 3.5 m/s, revealing solar-like oscillations. This is in general agreement with what we theoretically expect for this star. Samadi et al. (2005) predicts that the maximum observed oscillation amplitude $v_{\rm osc}$ scales as $(L/M)^{0.8}$. Using $v_{\rm osc,\odot} = 0.23$ m/s, $L/L_\odot = 59$ and $M/M_\odot$ between 2 and 2.8, we obtain a maximum oscillation amplitude between 2.6 m/s and 3.5 m/s, which is consistent with what we observe.

An analysis of the power spectrum, using auto-correlation and comb response techniques, reveals a large separation of either 4.8 μHz or its one-day alias 6.7 μHz. The case of 4.8 μHz seems somewhat stronger, but on the basis of the current dataset, we cannot exclude the 6.7 μHz possibility. Also both values are theoretically consistent with shell hydrogen-burning stellar models within the error box on the HR diagram. This ambiguity is related primarily to the uncertainty in modeling convection. For each of the large separations, we traced the principal peaks contributing to the auto-correlation and the comb response.

There is no compelling evidence in the dataset for more than one (independent) frequency spacing, which is consistent

with the results of Dziembowski et al. (2001) who predicted that for red giants non-radial modes should have a much lower amplitude than the radial ones. We cannot exclude, however, that some of the lower amplitude peaks that we considered now as noise may actually be frequency peaks of non-radial modes.

The uncertainty on the given frequency separations depends on the accuracy of the derived frequencies. This in turn depends partly on the damping time which is poorly known for red giants. Only for one red giant, ξ Hya, an attempt has been made to estimate the damping time (Stello et al. 2004). The large Monte Carlo simulations needed for such an estimate will be considered in the near future.

Acknowledgements. This research has made use of the SIMBAD database, operated at CDS, Strasbourg, France. Part of this work was supported financially by the Swiss National Science Foundation. J.D.R. is a postdoctoral fellow of the Fund for Scientific Research, Flanders. C.B., A.M. and C.A. were supported by the Research Fund K.U.Leuven under grant GOA/2003/04. We thank the anonymous referee for the careful reading of the manuscript.

References

Alexander, D. R., & Ferguson, J. W. 1994, ApJ, 437, 879
Baranne, A., Queloz, D., Mayor, M., et al. 1996, A&AS, 119, 373
Bessell, M. S., Castelli, F., & Plez, B. 1998, A&A, 333, 231
Blackwell, D. E., Petford, A. D., Arribas, S., Haddock, D. J., & Selby, M. J. 1990, A&A, 232, 396
Blackwell, D. E., & Lynas-Gray, A. E. 1998, A&AS, 129, 505
Bouchy, F., Pepe, F., & Queloz, D. 2001, A&A, 374, 733
Buzasi, D., Catanzarite, J., Laher, R., et al. 2000, ApJ, 532, L133
Christensen-Dalsgaard, J. 2004, Sol. Phys., 220, 137
Christensen-Dalsgaard, J., & Berthomieu, G. 1991, Solar interior and atmosphere (University of Arizona Press), 401
Decin, L., Vandenbussche, B., Waelkens, C., et al. 2003, A&A, 400, 709
Dziembowski, W. A., Gough, D. O., Houdek, G., & Sienkiewicz, R. 2001, MNRAS, 328, 601
Eyer, L., & Grenon, M. 1997, in Proc. of the ESA Symposium Hipparcos – Venice '97, ESA SP-402, 467
Flower, P. J. 1996, ApJ, 469, 355
Frandsen, S., Carrier, F., Aerts, C., et al. 2002, A&A, 394, L5
Hatzes, A. P., & Cochran, W. D. 1994, ApJ, 432, 763
Henyey, L., Vardya, M. S., & Bodenheimer, P. 1965, ApJ, 142, 841
Houdashelt, M. L., Bell, R. A., & Sweigart, A. V. 2000, AJ, 119, 1448
Houdek, G., & Gough, D. O. 2002, MNRAS, 336, L65
Iglesias, C. A., & Rogers, F. J. 1996, ApJ, 464, 943
Jorissen, A., Mowlavi, N., Sterken, C., & Manfroid, J. 1997, A&A, 324, 578
Kallinger, T., Zwintz, K., Pamyatnykh, A. A., et al. 2005, A&A, in press
Lejeune, T., & Schaerer, D. 2001, A&A, 366, 538
Morel, P. 1997, A&AS, 124, 597
Percy, J. R., & Shepherd, C. W. 1992, IBVS, 3792, 1
Perryman, M. A. C., Lindegren, L., Kovalevsky, J., et al. 1997, A&A, 323, 49
Rogers, F. J., & Nayfonov, A. 2002, ApJ, 576, 1064
Samadi, R., Georgobiani, D., Trampedach, R., et al. 2005, A&A, submitted
Stello, D., Kjeldsen, H., Bedding, T. R., et al. 2004, Sol. Phys., 220, 207
Taylor, B. J. 1999, A&AS, 134, 523